SANDIA REPORT
SAND2007-1560
Unlimited Release
Printed March 2007

Nanoporous Microbead Supported Bilayers: Stability, Physical Characterization, and Incorporation of Functional Transmembrane Proteins

Ryan W. Davis, Adrean Flores, Todd A. Barrick, Jason M. Cox, Susan M. Brozik, Gabriel P. Lopez and James A. Brozik

Prepared by
Sandia National Laboratories
Albuquerque, New Mexico 87185 and Livermore, California 94550

Sandia is a multiprogram laboratory operated by Sandia Corporation, a Lockheed Martin Company, for the United States Department of Energy's National Nuclear Security Administration under Contract DE-AC04-94AL85000.

Issued by Sandia National Laboratories, operated for the United States Department of Energy by Sandia Corporation.

Available to DOE and DOE contractors from
U.S. Department of Energy
Office of Scientific and Technical Information
P.O. Box 62
Oak Ridge, TN 37831

Telephone: (865) 576-8401
Facsimile: (865) 576-5728
E-Mail: reports@adonis.osti.gov
Online ordering: http://www.osti.gov/bridge

Available to the public from
U.S. Department of Commerce
National Technical Information Service
5285 Port Royal Rd.
Springfield, VA 22161

Telephone: (800) 553-6847
Facsimile: (703) 605-6900
E-Mail: orders@ntis.fedworld.gov
Online order: http://www.ntis.gov/help/ordermethods.asp?loc=7-4-0#online

SAND2007-1560
Unlimited Release
Printed March 2007

Nanoporous Microbead Supported Bilayers: Stability, Physical Characterization, and Incorporation of Functional Transmembrane Proteins

Ryan W. Davis †, Adrean Flores †, Todd A. Barrick†, Jason M. Cox †, Susan M. Brozik ‡, Gabriel P. Lopez + and James A. Brozik†

‡Biosensors and Nanomaterials, Sandia National Laboratories
†Department of Chemistry, University of New Mexico
+Department of Chemical and Nuclear Engineering, University of New Mexico

Abstract

The introduction of functional transmembrane proteins into supported bilayer-based biomimetic systems presents a significant challenge for biophysics. Among the various methods for producing supported bilayers, liposomal fusion offers a versatile method for the introduction of membrane proteins into supported bilayers on a variety of substrates. In this study, the properties of protein containing unilamellar phosphocholine lipid bilayers on nanoporous silica microspheres are investigated. The effects of the silica substrate, pore structure, and the substrate curvature on the stability of the membrane and the functionality of the membrane protein are determined. Supported bilayers on porous silica microspheres show a significant increase in surface area on surfaces with structures in excess of 10 nm as well as an overall decrease in stability resulting from increasing pore size and curvature. Comparison of the liposomal and detergent-mediated introduction of purified bacteriorhodopsin (bR) and the human type 3 serotonin receptor (5HT3R) are investigated focusing on the resulting protein function, diffusion, orientation, and incorporation efficiency. In both cases, functional proteins are observed; however, the reconstitution efficiency and orientation selectivity are significantly enhanced through detergent-mediated protein reconstitution. The results of these experiments provide a basis for bulk ionic and

fluorescent dye-based compartmentalization assays as well as single-molecule optical and single-channel electrochemical interrogation of transmembrane proteins in a biomimetic platform.

Contents

- bR Reconstitution.
- Functionality and Orientation of bR.
- 5HT3R Concentration, Orientation, and Function.
- Patch Clamp.

Figures

Tables

Introduction

The adsorption of proteoliposomes onto a solid substrate and subsequent supported bilayer formation was first demonstrated by Brian and McConnell over 20 years ago.[1] Since this discovery, a great deal of research interest has focused on the development of biomimetic supported bilayer systems incorporating various polymeric, ceramic, and functionalized substrates[2-11] for the introduction of membrane proteins for bio- and chemical sensing, drug discovery and delivery, and fundamental biophysical studies in near-native environments. Concurrently, advances in silica processing have made it possible to produce microspheres, monodispersed in size and surface characteristics,[4,12,13] which are now commercially available. It has recently been shown that membrane-associated proteins can be incorporated into lipid bilayers supported on silica beads.[4] In one such example, protein association with the membrane was observed to be coincident with macroscopic bead aggregation.[14] In another report, similar bilayer-coated beads were used to study phosphoinositide-specific phospholipase activity using laser trap-based microelectrophoresis.[15] Expansion of these capabilities through high throughput parallel and multiplex strategies offers great possibilities for biosensor technology;[16,17] however, functional reconstitution of complex transmembrane proteins into this platform has yet to be demonstrated.

Significant advances have been made in the basic understanding of the reversible saturation and subsequent solubilization of phospholipid bilayers using various nonionic detergents.[18-26] These results provide a physicochemical basis for the purification and functional reconstitution of complex transmembrane proteins into unilamellar vesicles. There are hundreds of studies on this subject, but a few noteworthy examples pertinent to this study include the proteotypical G-protein coupled receptor, bacteriorhodopsin (bR),[27] and a ligand-gated ion channel responsible for fast signal transduction, the serotonin receptor (5HT3R).[28] The introduction of solid supports, however, introduces many biophysical questions from the perspective of both the membrane and the incorporated protein. Among these questions are perturbations in membrane fluidity, the conditions for effective detergent solubilization and reconstitution, protein-substrate interactions, protein functionality, and controlling protein orientation. In general, the electrostatic and van der Waals forces of hydrophilic surfaces promote the formation of stable bilayers with lateral fluidity and impermeability to

ionic species.[4] However, in many supported bilayer systems, questions remain pertaining to the steric hindrance of supported bilayer formation resulting from proteins protruding from the proteoliposomal surface[29] and the inhibition of diffusion and protein function due to protein-substrate interactions.[30]

In an attempt to minimize these issues, silicon oxides have been suggested to be among the most consistent surfaces for bilayer formation using liposomal fusion.[4,5,31] In these materials, several persistent monolayers of water (~10 Å) reside between the bilayer and the surface, providing for free diffusion in both membrane leaflets and leaving long range interactions intact,[32-35] much like a natural biological membrane. The following article reports on the long-term stability, detergent solubilization, and protein incorporation in nanoporous microsphere supported bilayers (NMsb's) resulting from varying particle diameter and surface porosity. This study seeks to identify the optimal surface pore structure for minimal protein-substrate interaction and to gain a better understanding of the stability affects induced by curvature in rigid spherical supports.

In addition to traditional proteoliposome deposition, a method for introducing detergent-solubilized membrane proteins into preformed supported bilayers is described. A comparison of the two methods based upon the incorporation efficiency, orientation specificity, and functionality is also reported. Finally, micromanipulation and patch clamp electrochemical measurements were attempted on the NMsb's, and the cumulative results are discussed in terms of a comparison to biological cells and the potential use in biosensor applications, including receptor-based biodetection and signal amplification.

Materials and Methods

Characterization of Nanoporous Silica Microbeads. Pore Sizes and Bead Densities. Nucleodur and Nucleosil porous silica microspheres were purchased from GFS with the following parameters: 10, 20, and 30 μm diameter beads, each with 10 nm pores, and additional 10 μm beads with 50 and 100 nm pores. Scanning electron microscopy (SEM) images of the beads were taken with a Hitachi S-5200 NanoSEM. Aqueous hemacytometer counting of a known mass of each of the different bead types gave the number of the beads,

from which the density was calculated by determining the spherical volume per particle. For comparison to the hemacytometer result, a check of the density was also measured by a water displacement assay for a known mass of beads. The mass per bead was used to calculate the spherical surface area of an enveloping membrane. By using known values for the headgroup area of a specified phospholipid in its final hydrated bilayer phase,[36-38] the corresponding quantity of phospholipid necessary for coating the microspheres was calculated.

Solvent-Accessible Surface Area. In order to measure the total solvent-accessible surface area of a given set of beads, an octyltrichlorosilane (OTS)-based self-assembled monolayer (SAM) saturation experiment was performed. Dry beads were weighed and exposed to 10 mL of a warm (50 ºC) 0.5 M OTS solution in heptane. The beads were agitated gently for 15 min, centrifuged and washed with 1:1 $CHCl_3$/*n*-hexane. This process was repeated to vary the number of exposures from 0 to 5. After the final exposure cycle, the beads were washed a final time in $CHCl_3$ and dried under a nitrogen stream at 40 ºC with agitation for 48 h. The SAM-coated beads were then reweighed and dissolved in 10 mL of *n*-hexadecane. Five microliter aliquots of suspensions under stirring were delivered to a hemacytometer cell, and bead counting was performed to calculate the new SAM-coated bead mass. Assuming a close-packed SAM, the solvent-accessible surface could then be determined. As a check of the bead density, total surface area, and pore size and volume, nitrogen absorption measurements were performed using a Micromeritics ASAP 2010 physisorption analyzer.

Hydrophilic Surface Treatment of Nanoporous Silica Beads. Beads were weighed and washed in a 4% peroxide/4% ammonium hydroxide solution at 80-90 ºC for 10 min. The beads were then centrifuged and washed with Nanopure water and resuspended in a 4% peroxide/0.4 M HCl solution and heated to 80-90 ºC for 10 min. The beads were then centrifuged and washed three times with Nanopure water and suspended in an internal buffer solution containing fluorescent or ionic markers used in the following experiments.

Preparation of Small Unilamellar Vesicles (SUVs). Fluorescent and nonfluorescent phospholipids were purchased from Molecular Probes and Avanti Polar Lipids, respectively

[L-α-phosphatidylcholine (EPC); 1,2-dimyristoyl-*sn*-glycero-3-phosphocholine (DMPC); 1,2-dioleoyl-*sn*-glycero-3-phosphocholine (DOPC); 1,2-dioleoyl-*sn*-glycero-3-phosphoethanolamine (DOPE); 1,2-dipalmitoyl-*sn*-glycero-3-phosphocholine (DPPC); dihexadecyldimethylammonium bromide (DHDAB); 2-(4,4-difluoro-5,7-dimethyl-4-bora-3a,4a-diaza-*s*-indecene-3-doceanoyl-1-hexadecanoyl-*sn*-glycero-3-phosphocholine ($^{\beta}$-BODIPY FLC-HPC); Lissamine Rhodamine B 1,2-dihexadecanoyl-*sn*-glycero-3-phosphoethanolamine, triethylammonium salt (Lissamine Rhodamine DHPE)]. Before use, each was dissolved in chloroform and stored at -80 ºC for up to two weeks. For a given microsphere sample, a stoichiometric amount of phospholipids was calculated and a 100× molar excess of total phospholipid was added in the desired molar fractions to a round-bottom flask and dried under nitrogen. The resulting phospholipid cake was then further dried under vacuum for a minimum of 20 min. The phospholipid cake was then reconstituted (>1.5 mg/mL) in buffer solution at 50 ºC containing fluorescent or ionic markers used in the following experiments. Once the lipid cake was fully dissolved, the resulting liposome suspension was transferred to a Falcon tube and subjected to sonication using a Branson 250 ultrasonicator (microtip setting = 6, duty cycle = 20%) for 10 min at 4 ºC, at which point the turbidity was removed and unilamellar vesicles between 30 and 100 nm were formed.[53-54]

Purification of His_6-5HT3R from Human Embryonic Kidney (HEK) Cells. Purification of 5HT3R into proteomicelles was adapted from the work of Hovius et al.[39] Briefly, following selection, adherent HEK 293 cells expressing 5HT3R with C-terminal His tags were grown to 90-100% confluence, as described elsewhere.[40] The media was then decanted, and the cells were washed with 5 mL of 1× phosphate-buffered saline (PBS) buffer. Immediately following, the cells were exposed to 10 mL of 1× PBS with 1 mM EDTA for 10 min. The cells were then collected and centrifuged for 5 min at 1900 × g, and the buffer was decanted twice. The cells were then weighed and flash frozen in liquid nitrogen for storage at -80 ºC. All of the following purification steps were performed on ice or at 4 ºC. One gram of cell pellet was resuspended in 10 mL of 10 mM HEPES buffer, pH 7.4, containing 1 mM EDTA. The cells were then homogenized using an Ultra Turrax 18 at full speed (24 000 rpm). A 25 µL portion of protease inhibitor cocktail (P8849, Sigma Aldrich) was then added, and the pellet was diluted to twice its original volume by adding 10 mL of 1× PBS buffer. The

membrane pellet was then isolated by centrifuging in an Allegra 25R centrifuge at 20400 × g for 20 min followed by removal of the supernatant. The membrane pellet was then resuspended in 4 mL of HEPES buffer, pH 7.4, and vortexed briefly. A 200 μL portion of 50 mM C12E9 detergent (Fluka) was then added, and the solution was incubated for 1 h with gentle agitation. A 150 μL portion of Ni-NTA magnetic agarose beads (Qiagen; 3 mg/mL binding capacity) was combined with 1.5 mL of equilibration buffer (10 mM $NaPO_4$, 500 mM NaCl, 0.4 mM C12E9, 20 mM imidazole). Note: the packaging solvent was removed from the Ni-NTA magnetic agarose beads prior to use, and the beads were equilibrated for 1 h with gentle agitation. After removal of the equilibration buffer, the beads were then combined with the detergent-solubilized membrane pellet, 33 μL of 3 M imidazole was added, and the suspension was agitated overnight. On the following day, the beads were captured and washed five times with equilibration buffer. The receptor was then eluted three times with 500 μL of elution buffer (10 mM NaPO4, 500 mM NaCl, 0.4 mM C12E9, 250 mM imidazole) with agitation for 10 min between cycles. Final purification was performed by dialysis following reconstitution into liposomes or preformed supported bilayers. SDS-PAGE (10-20% gradient Tris-glycine, SYPRO ruby stain) was performed on all purification fractions following trichloroacetic acid extraction according to the method of Lemelli.[40,41] Fluorescent bands at 49 and 64 kD were observed in the elution fractions, indicating the presence of the glycolsylated and deglycosylated forms of 5HT3R.

Synthesis of Fluorescent Ni-NTA Conjugates. Fluorescent Ni-NTA conjugates were synthesized according to the work of Guignet et al.[42] Briefly, *N*-(5-amino-1-carboxypentyl)iminodiacetic acid (Aldrich) was dissolved in 0.1 M $NiCl_2$. The pH was adjusted to 8.0 with NaOH, and the solution was allowed to evaporate overnight yielding aquamarine crystals of Ni^{2+}-NTA-lysine. 5(6)-CR 6G SE and 5 equiv of Ni^{2+}-NTA-lysine were dissolved in 1:1 acetonitrile and 50 mM $NaHCO_3$, pH 9.0, and incubated with stirring for 12 h in the dark at 22 ºC. The product was purified by thin layer chromatography on silica gel 60 plates eluting with $CHCl_3/CH_3OH/H_2O$ = 66/25/4 (R_f = 0.21) and extracting with acetonitrile/ H_2O = 1/1. The product was then filtered and lyophilized for storage at -80 ºC until use.

Proteoliposome Preparation. bR purple membrane (labeled or unlabeled) was dissolved in 10 mM HEPES buffer, pH 6.0, containing 10 mM NaCl, 80 μM $MgCl_2$, and 20 μM $CaCl_2$. *n*-Octyl-$^{\beta}$-D-glucopyranoside (OG, Aldrich) was added in 6 (45.6 μL, 1 M) aliquots over 1 h at 35 ºC to create proteomicelles with a detergent-to-protein ratio of 40:1 (w/w). Concurrently, a liposome solution (95% mol/mol EPC, 5% mol/mol DOPE; final protein/phospholipid = 1:200-1:250 w/w) was warmed to 35 ºC, and the same detergent (OG) was added in 6 aliquots over 1 h to create detergent-saturated liposomes (0.024 M OG) with a detergent-to-phospholipid ratio of ~1:2. The bR proteomicelles were then added to the detergent-saturated liposomes, incubated at 35 ºC for 1 h, and stored overnight at room temperature. The resulting solution was then subjected to dialysis using a 15 kD cutoff dialysis cassette (Tube-O-DIALYZER, GBiosciences) submerged in 1 L of the buffer solution described above with washed SM2 BioBeads (BioRad) added to the external dialysis solution in three additions over 6 h as described previously.[43,44] A similar procedure was applied for nonaethylene glycol monododecyl ether (C12E9, Fluka)-solubilized His-tagged 5HT3R purified from HEK cells using a 25 kD cutoff dialysis cassette with BioBeads additionally added to the internal dialysis cassette buffer.

Fluorescence Labeling of bR. Fluorescence labeling of bR was adapted from the work of Kahya et al.[45] Briefly, following proteoliposome reconstitution, bR was exposed to three molar equivalents of 5(and 6)-carboxyrhodamine 6G succinimidyl ester (5(6)-CR 6G SE, Molecular Probes) in bicarbonate buffer at pH 8.5 for 1 h at 22 ºC followed by 16 h at 4 ºC. The resulting fluorescent protein conjugate was then purified to remove unreacted dye by dialysis using a 10 kD cutoff dialysis cassette in 1 L of 10 mM HEPES buffer (pH 7.4, with 10 mM NaCl, 80 μM $MgCl_2$, and 20 μM $CaCl_2$ with washed SM2 BioBeads).

Preparation of Nanoporous Microbead Supported Bilayers. The desired number of beads was pipetted with stirring from a stock suspension (10 μm: 1.25×10^8 beads/mL; 20 μm: 1.56×10^7 beads/mL; 30 μm: 4.63×10^6 beads/mL), and the supernatant was removed. The freshly prepared liposome or proteoliposome solution was then added, and the suspension was vortexed on the lowest setting for 45 min. The suspension was then allowed to sit undisturbed for 5 min. The beads were then centrifuged and washed with the desired

external buffer to remove phospholipids free in solution. Repeating the washing procedure three or more times was found to be sufficient to remove all phospholipids unincorporated into the supported bilayer.

Direct 5HT3R Reconstitution into NMsb's. A suspension of NMsb's (10 μm diameter, 10 nm pores) in 0.5 mL of 10 mM HEPES buffer was warmed to 35 ºC, and 25 mM C12E9 was added in 6 (1.5 μL) aliquots with stirring to adjust the detergent-to-phospholipid ratio to 1:2.2 over 1 h. 5HT3R was freshly purified as described above and combined with the detergent-saturated supported bilayers, so that the final detergent-to-phospholipid ratio did not exceed 3:2, and the overall detergent concentration was above the critical micelle concentration (cmc). The mixture was then further incubated at 35 ºC for 1 h with gentle agitation. The resulting bead suspension was then centrifuged and washed, and the remaining detergent was removed with SM2 BioBeads and dialysis as described above. For electrochemical measurements, the beads were exposed to 10 mM Ca^{2+} prior to NMsb formation, and, likewise, 10 mM Ca^{2+} was added to 1 L of 10 mM HEPES dialysis buffer. Following dialysis, the beads were centrifuged and washed three times with 10 mM HEPES buffer.

Asymmetric Supported Bilayer Formation. Samples of the SAM-coated microspheres described above were exposed to fluorescently labeled liposomes as well as 0.5% mol/mol Rhodamine DHPE and 95.5% mol/mol EPC as chloroform solutions. Liposome deposition was performed as described above. SAM exposed beads that had been exposed to phospholipids in chloroform were dried under nitrogen and washed with buffer five times.

Electrochemical Measurements. Bilayer stability, detergent solubilization, and protein functionality were probed using a calcium-sensitive electrode purchased from Microelectrodes, Inc. (MI-600 with MI-409F reference) and interfaced with an Orion voltmeter. In each experiment, the electrodes were positioned directly above the bed of bilayer-coated beads. Bilayer stability was assayed by loading the beads with 10 mM $CaCl_2$ followed by the daily recording of the external calcium concentration for 1 h. These experiments were carried out for different bilayer compositions, storage temperatures,

microsphere diameters, and porosities. The effect of detergent solubilization was probed by loading the beads as described above and recording the external calcium concentration resulting from exposure to varying detergent concentrations over the course of 1 h. The protein functionality of 5HT3R incorporated into NMsb's was assayed by loading the beads as described above and observing the change in external calcium concentration after exposure with varying concentrations of the 5HT3R agonist serotonin hydrochloride.

Fluorescence Measurements. Supported bilayer unilamellarity, stability, fusion, detergent solubilization, and surface area, as well as protein concentration, functionality, diffusion constants, and orientation were probed using a combination of techniques including fluorescence confocal imaging, UV-vis absorbance, and fluorimetry. Bilayer unilamellarity was probed by fluorescence intensity measurements resulting from the formation of NMsb's with 5% mol/mol Lissamine Rhodamine DHPE followed by exposure to 0.3 M KI quencher for 30 min. Bilayer stability was assayed by loading beads with 0.1 mM Rhodamine 6G followed by the daily recording of the absorbance and fluorescence intensities prior to buffer exchange. The fusion of SUVs with supported bilayers was assayed by repeatedly exposing fluorescent bead supported bilayers to an excess of fluorescent and nonfluorescent SUVs followed by UV-vis absorbance and confocal fluorescence imaging. The affect of detergent solubilization was assayed by adding 0.5% mol/mol of a fluorescently labeled membrane component (membrane and external labels) and measuring the fluorescence intensity of the supernatant resulting from exposure and 20 min equilibration to increasing concentrations of detergent. The affect of the surface structure (porosity) between the fluid and nonfluid bilayers was compared by adding 0.5% mol/mol of a fluorescently labeled membrane component and measuring the fluorescence intensity in bead number-matched samples. The orientation of bR was probed by fluorescence labeling of the extracellular portion of the protein followed by exposure to 0.3 M KI for 30 min. The total quenching efficiency for the solvent accessible dye used to label bR was found to be 95% at the concentration described. For 5HT3R quantification, a Ni-NTA fluorophore was used to reversibly bind to the C-terminal His tag for fluorescence emission measurements. Fluorescence recovery after photobleaching (FRAP) and confocal Z-scanning were performed using an inverted Nikon microscope (objective: Nikon 40×, NA 1.3, Apo) interfaced with a BioRad MRC-600 scan

head and 567 nm laser excitation. FRAP was used to assay the diffusion constant of dye compartmentalized in coated beads as well as the two-dimensional membrane diffusion of fluorescently labeled bR. The protein orientation of 5HT3R was determined by comparing the fluorescence intensities of Ni-NTA fluorophore labeled receptors that had been labeled before and after reconstitution into NMsb's. Protein function and orientation in bR was probed by loading beads with the pH-sensitive fluorophore SNARF-1 (Molecular Probes, Inc.), and monitoring the fluorescence spectrum during temperature-controlled exposure to a 100 W UV-filtered Xenon lamp.

Patch Clamp. Freshly prepared bilayer-coated microspheres were subjected to micromanipulation and patch clamp electrochemical analysis using an Axopatch 200B amplifier/headstage mounted on a home-built inverted microscope. Seal resistance and capacitance was monitored following the application of a 5 mV pulse for a variety of bead and tip conditions.

Results

Scanning Electron Microscopy. Figure 1 shows low (10 000×, 2.0 kV) and high (200 000× and 100 000×, 2.0 kV) magnification images of 10 μm diameter silica microspheres with different pore structures. The different pore sizes display regular and highly interconnected silica nanostructures that are self-consistent in morphology across the different size scales. The larger diameter (20 and 30 μm) beads with 10 nm pores show indistinguishable surface characteristics from the 10 μm, 10 nm porous beads under high magnification.

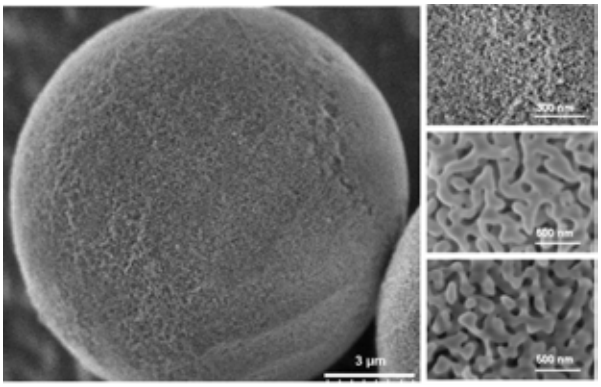

Figure 1. SEM images of silica microspheres with varying surface structure. Left: 10,000× image of a 10 μm bead with 10 nm pores. Right, descending vertically: 200,000× images of beads with 10 nm pores and 100,000× images of beads with 50 and 100 nm pores.

Density Measurements. Hemacytometer counting, water displacement, and nitrogen absorption assays were employed to determine the densities of the different bead types. The results of these measurements all agree within 5% of each other. Compared to bulk silica, the resulting density for the 10 nm porous beads suggests that the beads are ~42% empty space independent of the diameter. The beads with the larger pores (10 μm diameter, 50 and 100 nm pores), however, have higher densities, corresponding to ~20% empty space compared to bulk silica.

Microbead Surface Area Measurements. The results of gravimetric analysis and hemacytometer counting of bead samples allows for the determination of the SAM mass per bead upon exposure to OTS and gives a measure of the solvent-accessible surface area of the nanoporous beads. Figure 2 shows the results of density saturation analysis for a close-packed C-8 SAM. On the basis of recent experimental measurements for the determination of the surface area per molecule of a close-packed C-8 SAM on silica (20 $Å^2$),[46] the calculated microsphere surface areas were shown to be ~4 orders of magnitude higher than the surface area of an equivalent nonporous microbead. This value is decreased by ~30% in beads with 50 and 100 nm pores. Nitrogen absorption measurements show close agreement with the total surface area calculated by SAM saturation in this system. Additionally, SAM saturation in these experiments was shown to be dependent on the bead size, with the 10 μm beads requiring two exposures of OTS, the 20 μm beads requiring three exposures, and the 30 μm beads requiring four exposures.

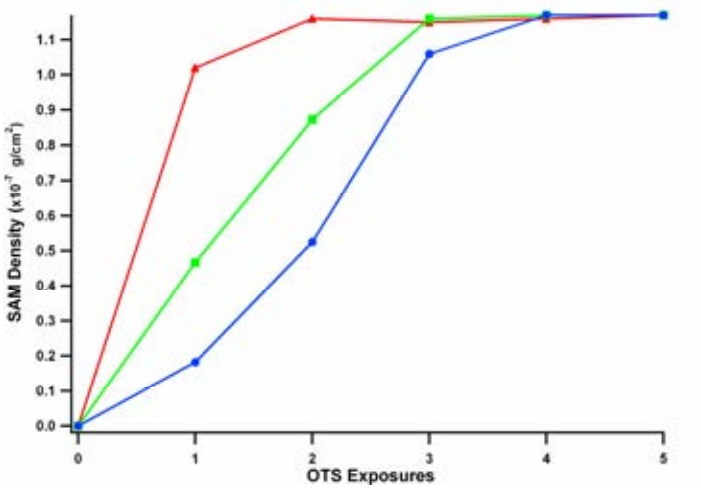

Figure 2. Gravimetric C-8 SAM density saturation on microbeads with various diameters, (▲) 10 μm, (■) 20 μm, and (●) 30 μm (10 nm pores), resulting from increasing numbers of OTS exposures. SAM saturation density is based on a calculated close-packed SiC_8 density of 1.17×10^{-7} g/cm^2.[46]

Dye Adsorption. The exposure of hydrophilically treated microspheres with Rhodamine 6G displayed spectral characteristics unchanged from those of buffer-solubilized dye. Daily fluorescence measurements following buffer exchange gave an adsorption half-life of ~4 days, independent of bead size and porosity. Confocal Z-scanning fluorescence microscopy revealed that the total concentration of fluorophore decreases near the center of the bead, with this effect being more pronounced in the larger pore size/higher density beads. R6G-exposed SAM-coated (i.e., hydrophobic) beads displayed a 20 nm blue-shift in the absorbance and a 10 nm blue-shift in the fluorescence emission maxima, with similar Z-scanning cross-sections to unexposed beads.

Unilamellar Supported Bilayers. Fluorescence quenching of supported bilayers doped with 5% mol/mol Lissamine Rhodamine DHPE showed a 50-56% decrease in fluorescence intensity following exposure to 0.3 M KI after 30 min. This result suggests that the supported bilayers on this platform are unilamellar by the ratio of quenched external solvent-accessible fluorophores versus unquenched nonexternal solvent-accessible fluorophores. Attempts to generate multilamellar supported bilayers by reexposure of NMsb's to 1-20× equiv of fluorescent SUVs were unsuccessful.

Bilayer Stability Measurements. The results of two long-term assays monitoring the release of R6G and Ca^{2+} under various storage conditions and bilayer compositions are summarized in Table 1. Several interesting observations are made as a result of this study. First, in each

Table 1. EPC Compartmentalization Half-Life of Internal Analytes in Days

	microbead size (10 nm pores)			pore structure (10 μm beads)		
	10 μm	20 μm	30 μm	10 nm	50 nm	100 nm
R6G[ab]	4.2	17.9	24.6	4.2	4.1	4.1
Ca^{2+} [b]	2.1	2.8	4.9	2.1	< 1.0	< 1.0
Ca^{2+} [c]	3.2	4.8		3.2	1.3	
Ca^{2+} [d]	3.3	4.9		3.3	1.6	

[a] R6G adsorption to uncoated silica beads = 4 days.[b] Stored at 21 ºC.[c] Stored at 4 ºC.[d] 5% mol/mol DHDAB, stored at 21 ºC.

case, the larger bead size corresponded to increased bilayer stability. Second, comparing the results from the calcium and dye release assays, a large increase in compartmentalization stability for the dye-loaded beads is indicated. This observation is believed to be the result of a combination of the strong adsorption of the dye to the bead, the destabilizing membrane potential created by loading the bead with Ca^{2+} ions, and the small size of the calcium ion and its large diffusion constant. Finally, lowering the storage temperature to 4 ºC or introducing 5% mol/mol of the positively charged lipid component, DHDAB, effectively doubled the stability half-lives. The effect of DHDAB is believed to be the result of an increase in the membrane-bead electrostatic bonding between the hydroxyl-rich (SiO^-) negatively charged microsphere surface and the positive charge introduced by DHDAB. Repeating this assay with the homogeneous phospholipids DMPC and DOPC produced a composition-dependent stability gradient. The stability half-lives were consistent on all surfaces and followed the order EPC > DOPC > DMPC. It is interesting to note that the order of the stabilities corresponds inversely to the order of the different lipids' gel-to-fluid phase transition temperatures (T_m), where T_m(EPC) = -10 ºC < T_m(DOPC) = 18.5 ºC < T_m(DMPC) = 22 ºC. Additionally, FRAP was performed on the internal volume of the coated beads of various sizes, which were loaded with R6G. Fluorescence recovery times of the internal volume of NMsb's indicate that the diffusion constant of dye molecules compartmentalized within the beads is identical for different bead sizes, indicating that the connectivity of the internal compartments is consistent among these samples.

Asymmetric Supported Bilayers. The formation of asymmetric bilayers was observed using confocal fluorescence Z-scanning microscopy. A bright ring of intensity was observed on the bead surface in both preparations, with the nonliposomal treatment producing higher fluorescence intensities than the bilayers generated by liposomal fusion. In both treatments, however, the fluorescence permeated deeper into the bead surface than beads coated with symmetrical bilayers. The overall yield of supported asymmetric bilayer formation was appreciably higher using nonliposomal methods due to the low suspendibility of SAM-exposed beads in aqueous media

Supported Bilayer Phospholipid Exchange with SUVs. The results of alternately reexposing bead supported bilayers to excess fluorescent and nonfluorescent SUVs are shown in Figure 3. In this assay, we observe a reversible exchange of phospholipids between SUVs and the supported bilayer. The large excess of SUVs used in this assay resulted in the bilayers taking on the fluorescent or nonfluorescent characteristic of the SUVs to which the bilayer was most recently exposed following several wash cycles. This observation demonstrates that SUV interactions with preformed NMsb's promote the exchange of bilayer components. This property thus allows for continuous modification of the supported bilayer and the possibility of recycling the supported bilayer substrate, for example, in flow cell-based devices; however, the generation of multilamellar bilayers by reexposing existing supported bilayers to SUVs was shown to be unsuccessful in this platform.

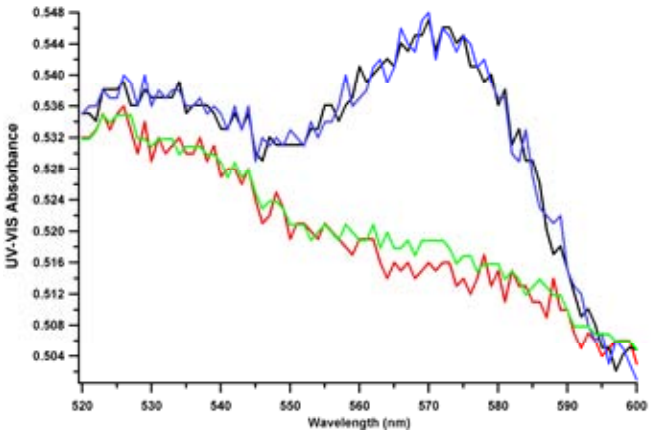

Figure 3. Reversible supported bilayer phospholipid exchange with excess SUVs. (red line) SUV exposure (1), PC with 0% mol/mol Rhodamine DHPE. (blue line) SUV exposure (2), PC with 1% mol/mol Rhodamine DHPE. (green line) SUV exposure (3), PC with 0% mol/mol Rhodamine DHPE. (black line) SUV exposure (4), PC with 1% mol/mol Rhodamine DHPE.

Bilayer Surface Area. Integrated fluorescence intensities of bead number-matched samples with varying pore sizes and phases are shown in Figure 4. The data are corrected for the relative difference in head group surface area between fluid-phase EPC (64 Å)[36] and gel-phase DPPC (46 Å).[37] Three notable observations from the data are (1) in both bead samples with pores above 10 nm, the surface area of the fluid (EPC) bilayers increases by 2-3×, (2) the surface area of gel-phase bilayers increases only slightly with increasing pore size, and (3) the surface areas of the gel and fluid bilayers are nearly identical in the smallest pore size, indicating a critical dimension for the invagination of fluid bilayers.

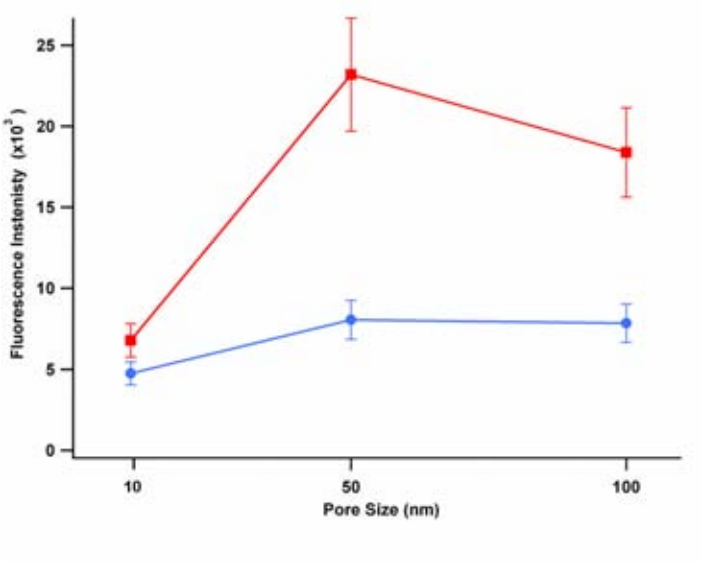

Figure 4. Relative surface areas of (■) EPC and (●) DPPC (each with 0.5% mol/mol Rhodamine DHPE) bilayers on 10 μm beads with varying pore structure. Fluorescence intensities are corrected for the EPC fluid-phase head group area versus the DPPC gel-phase head group area.

Supported Bilayer Detergent Solubilization. The results of the detergent-dependent calcium release assay are shown in Figure 5. Again we observe a significant curvature effect, with the lower curvature (larger bead size) supported bilayers being increasingly resistant to detergent disruption. The range of the ratios of detergent to phospholipid necessary for supported bilayer detergent saturation was determined to be ~0.16:1 for 10 μm, ~0.26:1 for 20 μm, and ~0.38:1 for 30 μm diameter microspheres. In a series of complementary experiments, fluorescence associated with labeled membrane components was measured as a function of increasing detergent concentration. NMsb's were prepared with either 0.5% mol/mol of fluorescently labeled membrane components $^{\beta}$-BODIPY FLC-HPC, in which the fluorophore is conjugated to one of the phospholipid tails, or 0.5% mol/mol Rhodamine DHPE, in which the fluorophore is conjugated to the phosphocholine head. In both cases, C12E9 detergent-saturated membranes remain associated with the bead scaffold up to 200:1 detergent/phospholipid (mol/mol, 50× cmc = 0.0001 M) at 35 ºC. In the case of OG, supported bilayer dissociation was observed at 75:1 detergent/phospholipid (mol/mol, 2× cmc = 0.0236 M) at 35 ºC. Although supported bilayer dissociation was shown to occur at high detergent-to-phospholipid ratio, at a detergent/phospholipid concentration of 1.5:1 (above the cmc), a qualitative change in the bilayer is observed for both detergents. At or above these concentrations, beads clump together, requiring vigorous stirring to obtain a homogeneous suspension. Above this ratio, the membrane is no longer intact as a supported bilayer (as shown by calcium release), but we observe the continued colocalization of

fluorescence with the bead by monitoring the UV-vis absorbance of the top solution after each 20 min equilibration time. We assert that this transition corresponds to Lichtenberg's[18] mid to late second stage of membrane solubilization, which is dominated by various mixed micelle and possibly bicelle structures.[47,48] A previous study, investigating the solubilization of planar supported bilayers using Triton-X, showed similar reversible solubilization above the cmc on a quartz substrate.[49]

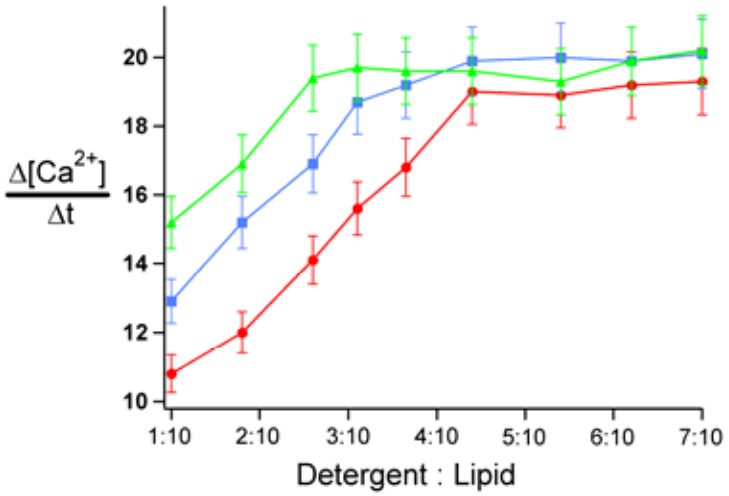

Figure 5. Supported bilayer detergent saturation for various bead diameters measured as calcium release: (▲) 10 μm, (■) 20 μm, and (●) 30 μm (10 nm pores). Calcium release was averaged over 1 h after exposure to C12E9. The calculated cmc in this experiment is coincident with 0.08 C12E9/EPC mol/mol.

bR Reconstitution. The results of a FRAP assay using fluorescently labeled bR NMsb's (10 μm diameter, 10 nm pores) produced by proteoliposome adsorption are shown in Figure 6. The results of this assay yield a diffusion constant of 0.038 $\mu m^2/s$ for light-adapted bR at low concentrations, which is within ~60% of that reported for bR in giant unilamellar vesicles (GUVs).[50] However, incomplete fluorescence recovery and the overall retention of the two-dimensional bleached area indicates the presence of mobile and immobile phases of the protein in the supported bilayer, consistent with the observations of Weng et al.[5] On the basis of the total ratio of the surface area bleached to the total bead surface area, the immobile phase is calculated to be ~10% of the incorporated bR. When comparing the above observed diffusion constant to the diffusion constant on beads with 50 and 100 nm pores, we observe a decrease in the measured effective diffusion constant by a factor of greater than 3. We believe this to be the result of the increasing degree of bilayer invagination on beads with larger pore size, thus increasing the total bilayer surface area and

substrate-protein interaction. This result is supported by bilayer surface area measurements, which show that the bilayer surface area is 2-3 times larger in the larger pore size beads.

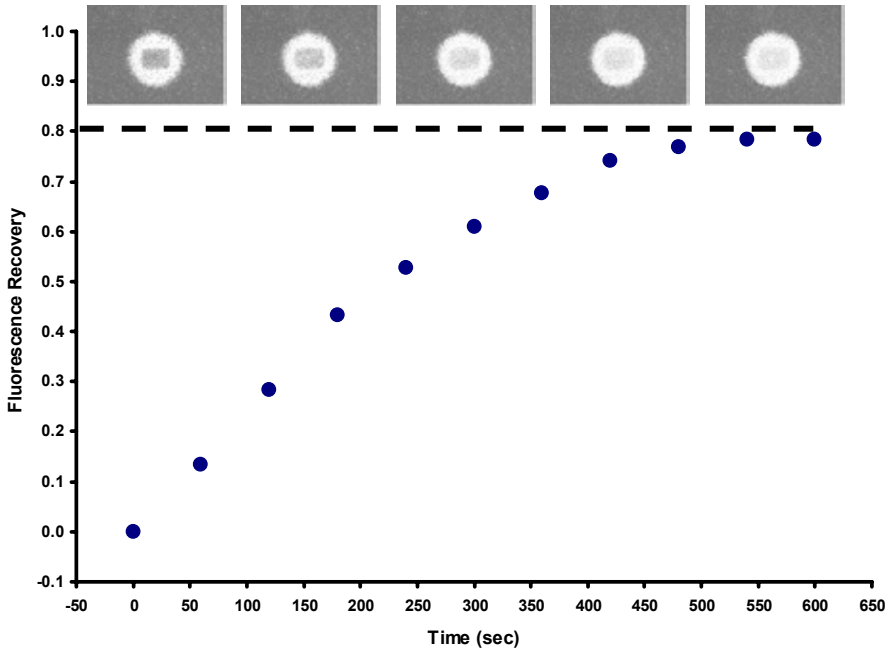

Figure 6. FRAP of 10 μm, 10 nm pore NMsb's containing 1:200-1:250 w/w fluorescently labeled bR/PL.

Functionality and Orientation of bR. It has been previously observed that bR inserts unidirectionally into preformed detergent-saturated SUVs.[27] Similar results were observed for bR reconstituted into detergent-saturated SUVs produced in our lab. Fluorescence spectra were recorded from beads that were loaded with 50 μM of the pH-sensitive dye, 5(and 6)-carboxy SNARF-1 before exposure to unlabeled bR proteoliposomes. Temperature-controlled (22 ºC) exposure to a 100 W UV-filtered Xenon lamp produced a small spectral shift under these conditions. A second measurement, in which 5 mM Gd^{3+} was added to the external solution, is shown in Figure 7. In this case, a large spectral shift is observed, corresponding to ~1.5 pH units, indicating the accumulation of a +90 mV membrane potential during illumination. In order to interrogate the orientation selectivity of bR in NMsb's incorporated by proteoliposomal deposition, a quenching assay was performed on extracellular fluorescence-labeled samples. As supported by the functionality assay, proteoliposome-deposited bilayers display 65% fluorescence quenching, indicative of 70% right-side-out-oriented bR, after correcting for the total quenching efficiency. From these observations, we propose the following mechanism of supported bilayer formation via

bR proteoliposomal fusion: unidirectionally aligned bR proteoliposomes interact with the microbead surface and experience liposome rupture to form at least two transient phospholipid structures that eventually adhere to the bead surface, resulting in 70% right-side-out protein alignment. Inhibition of non-right-side-out proteins in which the C-terminus is exposed to Gd^{3+} results in a net outward H^+ current under broad spectrum (500-750 nm) irradiation, resulting in the observed shift in the fluorescence spectrum.

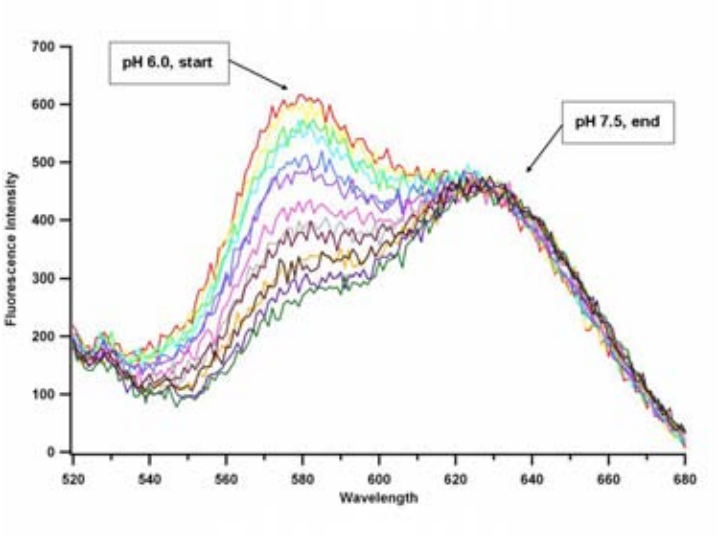

Figure 7. Time-dependent fluorescence spectra of SNARF-1-loaded NMsb's (10 μm diameter, 10 nm pores; 1:200-1:250 w/w bR/PL) under 488 nm excitation following consecutive 5 min exposures to a 100 W UV-filtered Xenon lamp.

In order to determine the effect of detergent saturation on the orientation selectivity of bR, extracellularly labeled bR containing NMsb's were exposed to saturating detergent conditions (0.024 M OG; 50:1 OG/PL), and the detergent was subsequently removed by either dialysis or repeated washing cycles. Fluorescence quenching after 30 min of exposure to KI showed 80% bleaching efficiency, corresponding to ~85% right-side-out orientation in both cases. However, in the washed samples, the overall starting fluorescence intensity was reduced significantly (~60%), indicating the resolubilization of a significant portion of bR resulting from detergent saturation.

5HT3R Concentration, Orientation, and Function. Upon completing detergent removal, fluorescence spectra of the 5HT3R-containing NMsb's were taken after exposure to 0.1 mM Ni-NTA-5(6)-CR 6G and three washings. These UV-vis spectra were corrected by titration with 0.1 mM EDTA and subtracting this baseline after three washes. Using a standard curve for Ni-NTA-5(6)-CR 6G, the final 5HT3R concentrations were measured to be ~15 nM for

the direct incorporation of 5HT3R and ~200 pM for proteoliposome deposition of 5HT3R. These concentrations correspond to a minimum of 7500 receptors per bead and 100 receptors per bead, respectively, from 1 g of starting HEK cells. This result is expected due to the large excess of proteoliposomes necessary to form a complete bilayer over a large curved surface. In order to probe the orientation of the receptors, an assay was conducted in which receptors were labeled before *and* after reconstitution, whereas other samples were either labeled before *or* after reconstitution. The results of this assay show a significant (74%) selectivity for the right-side-out alignment for proteoliposome deposited membranes that had been prepared in solubilizing detergent concentrations (detergent/lipid = 2.3:1, above the cmc). This result is believed to primarily be the result of the large steric hindrance of liposome fusion from the extracellular portion of 5HT3R. Performing the same assay for receptors reconstituted into preformed detergent-saturated supported bilayers resulted in a much higher (94%) degree of right-side-out alignment, which is believed to be the result of the supported bilayer's adherence to the surface of the bead combined with the large energy barrier for crossing the membrane of the large extracellular portion of 5HT3R. Results of the 5HT-induced calcium release functionality assay are shown in Figure 8. The sharp increase in calcium release versus controls from receptor-containing NMsb's when exposed to the 5HT3R agonist, serotonin hydrochloride, are indicative of the ligand-gated ion channel function in this system.

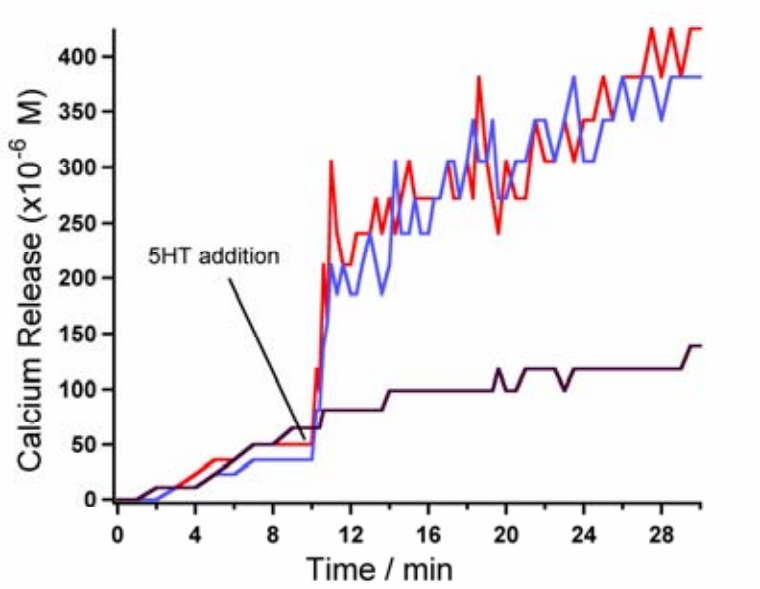

Figure 8. Functionality assay for NMsb's (10 µm diameter, 10 nm pores) with reconstituted 5HT3R under exposure to (black line) 0 µM, (blue line) 20 µM, and (red line) 200 µM serotonin hydrochloride.

Patch Clamp. Gigaseals were not observed on NMsb's on any of the range of bead sizes or pore structures using coated and uncoated (D-lysine, PDMS, OTS SAM) glass apertures ranging from 500 nm to 10 μm. However, translocation and micropositioning of NMsb's were performed using micropipettes incorporating pressure-controlled micromanipulation. This result suggests the importance of cellular flexibility in the formation of gigaseals for single-channel and whole-cell patch clamp electrochemical measurements. For these applications, less rigid supports such as polymeric hydrogels or multilamellar supported bilayers are proposed as a future direction for biomimetic investigation using patch clamp electrochemistry.

Discussion

Several noteworthy observations were made in probing the effects of substrate pore size and diameter in phosphocholine supported bilayers. With respect to curvature, the larger diameter beads displayed the greatest capacity to maintain compartmentalized fluorescent dye and calcium ions and were the most resistant to detergent solubilization. The conclusion that high curvature in phosphocholine supported bilayer systems can significantly reduce the resulting bilayer stability suggests the potential significance of the intrinsic curvature[51] of the incorporated bilayer components. Thus, adjusting the lipid component mixture to more efficiently match the curvature of a specified supported bilayer system may offer a large increase in bilayer stability. When considering pore size, it was observed that, in bilayers with pores $\leq$2 times the bilayer thickness, fluid bilayers span surface structures much like a bilayer in its gel phase. When the pore sizes are much larger than the bilayer thickness, the membrane is significantly invaginated into the pore, thus increasing the membrane surface area. For various applications, different degrees of invagination may be appropriate; however, the fraction of membrane-bound protein exposed to the surface may be significantly increased and the overall bilayer stability diminished.

In probing detergent solubilization, exposure of porous bead supported bilayers to increasing detergent concentrations showed reversible detergent *saturation* of the bilayer; however, even at detergent/phospholipid ratios exceeding 50:1 (above the cmc), complete bilayer solubilization was not observed. To rule out the possibility of perturbations resulting from

surface-accessible fluorescent tags, the experiment was repeated with an in-membrane fluorescent label with the same result. The evidence suggests, however, that the platform described is not a case of a detergent-resistant bilayer as seen in many biological systems,[52] but possibly the result of the high surface area for mixed micelle adsorption. Finally, protein reconstitution into preformed supported bilayers was carried out at detergent saturating conditions and resulted in a large increase in reconstitution efficiency and orientation selectivity.

Conclusion

Over the last several decades, membrane-bound proteins have become recognized as a major target for therapeutic and biosensing technologies. Interfacing these biological structures with synthetic materials thus offers an important challenge for the realization of future innovations. In order to overcome commonly observed artifacts resulting from the secondary interaction of transmembrane proteins with their synthetic substrates, supported phosphocholine bilayers on nanoporous silica microbeads were investigated at a range of sizes common to biological cells. Additionally, two methods of functional protein incorporation were demonstrated for comparison in vivo.

The results of these experiments provide a basis for ionic and fluorescent dye-based compartmentalization assays as well as high-resolution optical and electrochemical interrogation such as laser trapping and patch clamp. The structural stability added to the bilayer as a result of the porous substrate allows proteins to be incorporated using traditional nonionic detergent-based methods. Additionally, the availability of uniformly sized beads with uniform pore structure allows the bilayer diameter and surface area to be directly controlled. These findings demonstrate that bilayer-coated porous silica beads offer a stable, size selective, and convenient platform for the study and incorporation of purified transmembrane-bound proteins with minimal unfavorable protein-substrate interaction due to high surface porosity with $\leq$10 nm scale surface structures.

References

1. Brian, A. A.; McConnell, H. M. *Proc. Natl. Acad. Sci. U.S.A.* **1984**, *81*, 6159-6163.

2. Tanaka, M.; Sackmann, E. *Nature* **2005**, *437*, 656-663.

3. Anrather, D.; Smetazko, M.; Saba, M.; Alguel, Y.; Schalkhammer, T. J. *Nanosci. Nanotechnol*. **2004**, *4*, 1-22.

4. Buranda, T.; Huang, J.; Ramarao, G. V.; Ista, L. K.; Larson, R. S.; Ward, T. L.; Sklar, L. A.; Lopez, G. P. *Langmuir* **2003**, *19*, 1654-1663.

5. Weng, K. C.; Stalgren, J. J. R.; Duval, D. J.; Risbud, S. H.; Frank, C. W. *Langmuir* **2004**, *20*, 7232-7239.

6. Worsfold, O.; Voelcker, N. H.; Nishiya, T. *Langmuir* **2006**, *22*, 7078-7083.

7. Mornet, S.; Lambert, O.; Duguet, E.; Brisson, A. *Nano Lett.* **2005**, *5*, 281-285.

8. Geissbuehler, I.; Hovius, R.; Martinez, M. A.; Thampi, R.; Vogel, H. *Angew. Chem., Int. Ed.* **2005**, *44*, 1388-1392.

9. Römer, W.; Steinem, C. *Biophys. J.* **2004**, *86*, 955-965.

10. Ng, C. C.; Cheng, Y.-L.; Pennefather, P. S. *Biophys. J.* **2004**, *87*, 323-331.

11. Kiyofumi, K.; Hashizume, M.; Kikuchi, J.-I.; Taketani, Y.; Murakami, M. *Colloids. Surf., B: Biointerfaces* **2004**, *38*, 149-153.

12. Brinker, C. J.; Lu, Y.; Sellinger, A.; Fan, H. *Adv*. *Mater*. **1999**, *11*, 579.

13. Alonso, B.; Douy, A.; Veron, E.; Perez, J.; Rager, M. N.; Massiot, D. *J. Mater. Chem.* **2004**, *14*, 2006-2016.

14. Baksh, M. M.; Jaros, M.; Groves, J. T. *Nature* **2004**, *427*, 139-141.

15. Galneder, R.; Kahl, V.; Arbuzova, A.; Rebecchi, M.; Rädler, J. O.; McLaughlin, S. *Biophys. J.* **2001**, *80*, 2298-2309.

16. Loidl-Stahlhofen, A.; Schmitt, J.; Noller, J.; Hartmann, T.; Brodowsky, H.; Schmitt, W.; Keldenich, J. *Adv. Mater.* **2001**, *13*, 1829-1834.

17. Yingyongnarongkul, B. E.; How, S. E.; Diaz-Mochon, J. J.; Muzerelle, M.; Bradley, M. *Comb. Chem. High Throughput Screening* **2003**, *6*, 577-587.

18. Lichtenberg, D. *Biochim. Biophys. Acta* **1985**, *821*, 470-478.

19. Levy, D.; Gulik, A.; Seigneuret, M.; Rigaud, J.-L. *Biochemistry* **1990**, *29*, 9480-9488.

20. De la Maza, A.; Parra, J. L. *Colloid Polym. Sci.* **1994**, *272*, 721-730.

21. Otten, D.; Löbbecke, L.; Beyer, K. *Biophys. J.* **1995**, *68*, 584-597.

22. Wenk, M. R.; Alt, T.; Seelig, A.; Seelig, J. *Biophys. J.* **1997**, *72*, 1719-1731.

23. Kragh-Hansen, U.; le Maire, M.; Møller, J. V. *Biophys. J.* **1998**, *75*, 2932-2946.

24. Gliss, C.; Casalta, H.; Bayerl, T. M. *J. Phys. Chem. B* **1999**, *103*, 8908-8914.

25. le Maire, M.; Champeil, P.; Møller, J. V. *Biochim. Biophys. Acta* **2000**, *1508*, 86-111.

26. Ollivon, M.; Lesieur, S.; Grabielle-Madelmont, C.; Paternostre, M. *Biochim. Biophys. Acta* **2000**, *1508*, 34-50.

27. Rigaud, J.-R.; Paternostre, M.-T.; Bluzat, A. *Biochemistry* **1988**, *27*, 2677-2688.

28. Lummis, S. C. R.; Martin, I. L. *Mol. Pharmacol.* **1991**, *41*, 18-23.

29. Granéli, A.; Rydström, J.; Kasemo, B.; Höök, F. *Langmuir* **2003**, *19*, 842-850.

30. Wagner, M. L.; Tamm, L. K. *Biophys. J.* **2000**, *79*, 1400-1414.

31. Groves, J. T.; Ulman, N.; Boxer, S. G. *Science* **1997**, *275*, 651-653.

32. Bayerl, T. M.; Bloom, M. *Biophys. J.* **1990**, *58*, 357-362.

33. Johnson, S. J.; Bayerl, T. M.; McDermott, D. C.; Adam, G. W.; Rennie, A. R.; Thomas, R. K.; Sackmann, E. *Biophys. J.* **1991**, *59*, 289-294.

34. Koenig, B. W.; Krueger, S.; Orts, W. J.; Majkrzak, C. F.; Berk, N. F.; Silverton, J. V.; Gawrisch, K. *Langmuir* **1996**, *59*, 289-294.

35. Davis, R. W.; Patrick, E. L.; Meyer, L. A.; Ortiz, T. P.; Marshall, J. A.; Keller, D. J.; Brozik, S. M.; Brozik, J. A. *J. Phys. Chem. B* **2004**, *108*, 15364-15369.

36. McIntosh, T. J.; Magid, A. D.; Simon, S. A. *Biochemistry* **1989**, *28*, 7904-7912.

37. Wiener, M. C.; Suter, R. M.; Nagle. J. F. *Biophys. J.* **1989**, *55*, 315-325.

38. Kučerka, N.; Liu, Y.; Chu, N.; Petrache, H. I.; Tristram-Nagle, S.; Nagle, J. F. *Biophys. J.* **2005**, *88*, 2626-2637.

39. Hovius, R.; Tairi, A.-P.; Blasey, H.; Bernard, A.; Lundstrom, K.; Vogel, H. *J. Neurochem.* **1998**, *70*, 824-834.

40. Brozik, S. M.; Patrick, E. L.; Flemming, J. H.; Bachand, G. D.; Frink, L. J. D.; Brozik, J. A.; Davis, R. W.; Meyer, L. A.; Ortiz, T. P.; Marshall, J. A.; Keller, J. D. *SAND2004-5585*; Sandia National Laboratory: Albuquerque, NM, 2004; pp 31-40.

41. Lemelli, U. K. *Nature* **1970**, *227*, 680-685.

42. Guignet, E. G.; Hovius, R.; Vogel, H. *Nat. Biotechnol.* **2004**, *22*, 440-444.

43. Holloway, P. W. *Anal. Biochem.* **1973**, *53*, 304-308.

44. Levy, D.; Bluzat, A.; Seigneuret, M.; Rigaud, J. L. *Biochim. Biophys. Acta* **1990**, *1025*, 179-190.

45. Kahya, N.; Pécheur, E.-I.; de Boeij, W. P.; Wiersma, D. A.; Hoekstra, D. *Biophys. J.* **2001**, *81*, 1464-1474.

46. Gao, W.; Reven, L. *Langmuir* **1995**, *11*, 1860-1863.

47. Funari, S. S.; Nuscher, B.; Rapp, G.; Beyer, K. *Proc. Natl. Acad. Sci. U.S.A.* **2001**, *98*, 8938-8943.

48. Glover, K. J.; Whiles, J. A.; Wu, G.; Yu, N.-j.; Deems, R.; Struppe, J. O.; Stark, R. E.; Komives, E. A.; Vold, R. R. *Biophys. J.* **2001**, *81*, 2163-2171.

49. Csúcs, G.; Ramsden, J. J. *Biochim. Biophys. Acta* **1998**, *1369*, 304-308.

50. Kahya, N.; Wiersma, D. A.; Poolman, B.; Hoekstra, D. *J. Biol. Chem.* **2002**, *277*, 39304-39311.

51. Epand, R. M.; Epand, R. F. *Biophys. J.* **1994**, *66*, 1450-1456.

52. Schuck, S.; Honsho, M.; Ekroos, K.; Shevcenko, A.; Simons, K. *Proc. Natl. Acad. Sci. U.S.A.* **2003**, *100*, 5795-5800.

53. Ruysschaert, T.; Germain, M.; da Silva Gomes, J. F. P; Fournier, D.; Sukhorukov, G. B.; Meier, W.; Winterhalter, M. *IEEE Trans. Nanobiosci.* **2004**, *3*, 49-55.

54. Gregodiadis, G. *Liposomes as Drug Carriers*; Wiley: Chichester, U.K., 1988.

Distribution

1	MS 0123	Donna Chavez, 1011
2	MS 9018	Central Technical Files, 8944
2	MS 0899	Technical Library, 4536